A Fully Digitized Field-Oriented Controlled Induction Motor Drive Using Only Current Sensors

Lazhar Ben-Brahim, *Member, IEEE,* and Atsuo Kawamura, *Member, IEEE*

***Abstract*—A field-oriented control method based on predictive observer with a digital current regulation of induction motor, without speed and voltage sensors, is proposed. Measuring only stator currents, and estimating motor speed and rotor fluxes by a predictive state observer with variable poles selection, the stator currents are controlled to be exactly equal to the reference currents at every sampling instant. As a result, the speed and rotor fluxes are estimated with low sensitivity to parameters variation, and the torque ripples are reduced. The proposed method consists of four parts: 1) identification of the rotor speed, 2) derivation of a digital control law, 3) construction of a state observer that predicts the rotor flux and the stator currents; and 4) derivation of field-oriented control. This paper describes a theoretical analysis, computer simulations, and experimental results.**

I. Introduction

The field-oriented control system uses an electromechanical speed transducer coupled to the motor shaft to measure the rotor speed. The transducer encumbers the mechanical drive, and spoils the general characteristics of ruggedness and mechanical simplicity of the induction motor drive. From this regard, a speed sensorless system is preferred. Many kinds of induction motor drive systems, without speed sensor, have so far been proposed [1-4].

In this paper, a fully digitized field-oriented controlled induction motor drive using only current sensors is proposed. First, the stator flux is estimated to identify the rotor speed with low sensitivity to parameters variation [12]. Second, based on the estimated speed, the predictive discrete-time state observer estimates the rotor flux with lower sensitivity to parameters variation than the conventional slip frequency vector control. Finally, under the field-oriented control, the deadbeat technique is applied for the stator current regulation, resulting in low ripples of current and torque with relatively low switching frequency [9]-[11]. A low-power experimental setup was constructed using a fully digitized controller based on a digital signal processor (DSP) with the switching frequency of 1200 Hz. Simulation and experimental results proved the superiority of the proposed method over the conventional schemes, and therefore contributed to performance improvement of conventional vector control.

Manuscript received April 2, 1991; revised February 27, 1992.

L. Ben-Brahim is with the Heavy Apparatus Engineering Laboratory, Toshiba Corporation, Fuchu, Tokyo 183, Japan.

A. Kawamura is with the Department of Electrical and Computer Engineering, Yokohama University, Yokohama 240, Japan.

IEEE Log Number 9108311.

Section II gives the rotor speed identification scheme. The sampled-data model of voltage source inverter fed induction motor drive is presented in Section III. The design of predictive state observer is described in Section IV. Section V presents the proposed field-oriented controller using only current sensors. The digital computer simulation and the experimental results are given in Sections VI and VII, respectively. Finally, Section VIII concludes this paper.

II. Rotor Speed Identification

A. Conventional Speed Calculation Method

There are two different equations to estimate the rotor flux [1],

$$\dot{\lambda}_r = \frac{L_r}{L_m}(v_s - R_s i_s - \sigma L_s \dot{i}_s) \tag{1}$$

and

$$\dot{\lambda}_r = \left(\frac{-1}{T_r} I + \omega_r J\right)\lambda_r + \frac{L_m}{T_r} i_s. \tag{2}$$

All symbols are defined below (13). Equation (1) does not contain the rotor speed ω_r; however, (2) does. Thus, using these two equations, the rotor speed ω_r can be estimated. First, the electrical angle θ of the rotor flux vector is defined as follows:

$$\theta = \tan^{-1}\left(\frac{\lambda_{qr}}{\lambda_{dr}}\right) \tag{3}$$

The derivative of the above equation gives

$$\omega = \dot{\theta} = \frac{\lambda_{dr}\dot{\lambda}_{qr} - \lambda_{qr}\dot{\lambda}_{dr}}{\lambda_{dr}^2 + \lambda_{qr}^2}. \tag{4}$$

Then, substituting for $\dot{\lambda}_{dr}$ and $\dot{\lambda}_{qr}$ from (2), we obtain

$$\omega_r = \omega - \frac{L_m}{T_r}\frac{(i_{qs}\lambda_{dr} - i_{ds}\lambda_{qr})}{\lambda_{dr}^2 + \lambda_{qr}^2}. \tag{5}$$

Equation (5) indicates that the instantaneous rotor speed ω_r can be obtained using the rotor flux estimated in (1). There are two problems related to the rotor flux estimation based on (1): the need of an ideal integral and its sensitivity to parameters variation, especially stator resistance R_s, which has a strong effect at very low speed. It is known that this kind of speed estimation works without failure above 10% of the synchronous speed [6].

The literature on the speed estimation rarely used this method to identify the rotor speed, instead, all the calcula-

0278-0046/92$03.00

tions are made in the rotating reference frame. This method is sensitive to all parameters present in (1) and (5).

B. Speed Identification Based on Stator Flux

To estimate the speed in a simple way and to reduce the parameter sensitivity, the stator flux is used instead of rotor flux. Furthermore, stator voltages are estimated rather than measured. Therefore, only current sensors are used for the following method. First, the stator flux, $\boldsymbol{\lambda}_s$ is estimated by [5]:

$$\hat{\boldsymbol{\lambda}}_s = \int (\boldsymbol{v}_s - R_s \boldsymbol{i}_s)\, dt \tag{6}$$

where

$$\hat{\boldsymbol{\lambda}}_s = [\hat{\lambda}_{ds}, \hat{\lambda}_{qs}]^T$$

Second, the stator angle is defined as follows:

$$\theta = \tan^{-1}\left(\frac{\hat{\lambda}_{qs}}{\hat{\lambda}_{ds}}\right). \tag{7}$$

Third, the synchronous speed ω is estimated by the derivative of (7):

$$\hat{\omega} = \dot{\theta} = \frac{\hat{\lambda}_{ds}\dot{\hat{\lambda}}_{qs} - \hat{\lambda}_{qs}\dot{\hat{\lambda}}_{ds}}{\hat{\lambda}_{ds}^2 + \hat{\lambda}_{qs}^2} \tag{8}$$

Fourth, (8) is transformed into the sampled-data model using the first-forward difference approximation as follows:

$$\hat{\omega}(k) = \frac{\hat{\lambda}_{ds}(k-1)\hat{\lambda}_{qs}(k) - \hat{\lambda}_{qs}(k-1)\hat{\lambda}_{ds}(k)}{T(\hat{\lambda}_{ds}^2 + \hat{\lambda}_{qs}^2)}. \tag{9}$$

Note that (9) has a modeling error which, in turn, produces an error in the rotor speed estimation. However, this effect is removed by the use of a low-pass filter. Since the slip speed can be estimated by the torque reference Te^* and the rotor flux reference $|\lambda_r^*|$:

$$\omega_s^* = \frac{4R_r}{3P}\frac{Te^*}{(|\lambda_r^*|)^2} \tag{10}$$

the rotor speed $\hat{\omega}_r(k)$ is given by

$$\hat{\omega}_r(k) = \hat{\omega}(k) - \omega_s^*. \tag{11}$$

As Fig. 1 shows, this estimation is insensitive to the term σL_s and L_r/L_m. The drawback is that the effect of stator resistance R_s is strong around the very low speed range.

III. Digital Control Theory

A. Induction Motor State Equation

The basic equations of an induction motor with the d–q coordinates fixed to the stator are expressed as

$$\begin{bmatrix} \dot{\boldsymbol{i}}_s \\ \dot{\boldsymbol{\lambda}}_r \end{bmatrix} = \begin{bmatrix} A_{11} & A_{12} \\ A_{21} & A_{22} \end{bmatrix}\begin{bmatrix} \boldsymbol{i}_s \\ \boldsymbol{\lambda}_r \end{bmatrix} + \begin{bmatrix} B_1 \\ 0 \end{bmatrix}\boldsymbol{v}_s = A\begin{bmatrix} \boldsymbol{i}_s \\ \boldsymbol{\lambda}_r \end{bmatrix} + B\boldsymbol{v}_s. \tag{12}$$

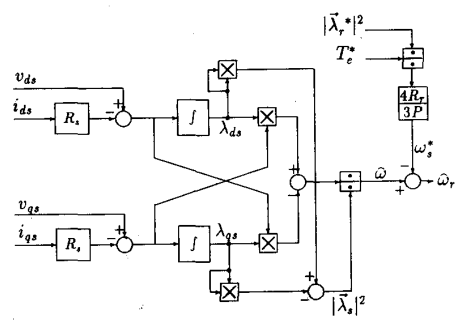

Fig. 1. Block diagram of stator flux based rotor speed identification.

The output equation is

$$\boldsymbol{i}_s = [I \quad 0]\begin{bmatrix} \boldsymbol{i}_s \\ \boldsymbol{\lambda}_r \end{bmatrix} = C\begin{bmatrix} \boldsymbol{i}_s \\ \boldsymbol{\lambda}_r \end{bmatrix}. \tag{13}$$

The symbol "$\cdot$" denotes the time derivative.

where

$$\boldsymbol{i}_s \triangleq \begin{bmatrix} i_{ds} \\ i_{qs} \end{bmatrix} \quad \boldsymbol{\lambda}_r \triangleq \begin{bmatrix} \lambda_{dr} \\ \lambda_{qr} \end{bmatrix} \quad \boldsymbol{v}_s \triangleq \begin{bmatrix} v_{ds} \\ v_{qs} \end{bmatrix}$$

$$A_{11} \triangleq -\left(\frac{R_s}{\sigma L_s} + R_r\frac{1-\sigma}{\sigma L_r}\right)I$$

$$A_{12} \triangleq -\frac{L_m}{\sigma L_s L_r}\left(-\frac{R_r}{L_r}I + \omega_r J\right)$$

$$A_{21} \triangleq L_m\frac{R_r}{L_r}I$$

$$A_{22} \triangleq -\frac{R_r}{L_r}I + \omega_r J$$

$$B_1 \triangleq \frac{1}{\sigma L_s}I$$

$$I \triangleq \begin{bmatrix} 1 & 0 \\ 0 & 1 \end{bmatrix} \quad J \triangleq \begin{bmatrix} 0 & -1 \\ 1 & 0 \end{bmatrix}$$

The meanings of the parameters are as follows.

R_s, R_r = stator and rotor resistances

L_s, L_r = stator and rotor self-inductances

L_m = stator/rotor mutual inductance

$\sigma \triangleq 1 - \frac{L_m^2}{L_s L_r}$ = leakage coefficient

ω_r = electrical rotor angular velocity

v_{ds}, v_{qs} = d-axis and q-axis stator voltages

i_{ds}, i_{qs} = d-axis and q-axis stator currents

λ_{dr}, λ_{qr} = d-axis and q-axis rotor fluxes

B. Deadbeat Control Law

Fig. 2 shows the proposed digital control system of the induction motor drive. Assuming that the inverter is for relatively high power application, a 1.8-kHz sampling frequency is chosen. To derive a sampled-data model of (12) and (13), inverter output voltages v_{ab}, v_{bc}, and v_{ca} are chosen as one or two voltage pulses of magnitude $+E$ or $-E$, satisfying the relation of $v_{ab} + v_{bc} + v_{ca} = 0$ at any moment as shown in Fig. 3. $\Delta T_{ab}(k)$, $\Delta T_{bc}(k)$, $\Delta T_{ca}(k)$ are the pulse widths of v_{ab}, v_{bc}, and v_{ca}, respectively, in the kth sampling. The two-phase pulse widths $\Delta T_d(k)$ and $\Delta T_q(k)$ are given by (14).

$$\begin{bmatrix} \Delta T_d(k) \\ \Delta T_q(k) \end{bmatrix} = \frac{2}{3} \begin{bmatrix} \frac{1}{2} & 0 & \frac{-1}{2} \\ 0 & \frac{\sqrt{3}}{2} & 0 \end{bmatrix} \begin{bmatrix} \Delta T_{ab}(k) \\ \Delta T_{bc}(k) \\ \Delta T_{ca}(k) \end{bmatrix}. \quad (14)$$

As long as these pulses are symmetrical at the center of the sampling interval, so are v_{ds} and v_{qs}, and assuming that the rotor speed is constant during a sampling interval T, the sampled-data model of (12) and (13) becomes

$$\begin{bmatrix} i_s(k+1) \\ \lambda_r(k+1) \end{bmatrix} = \begin{bmatrix} F_{11} & F_{12} \\ F_{21} & F_{22} \end{bmatrix} \begin{bmatrix} i_s(k) \\ \lambda_r(k) \end{bmatrix} + \begin{bmatrix} H_1 \\ H_2 \end{bmatrix} \Delta T(k)$$

$$= F \begin{bmatrix} i_s(k) \\ \lambda_r(k) \end{bmatrix} + H \Delta T(k) \quad (15)$$

where,

$$F \triangleq e^{AT}$$

$$H \triangleq e^{\frac{AT}{2}} BE$$

$$\Delta T(k) \triangleq [\Delta T_d(k), \Delta T_q(k)]^T.$$

F_{11}, F_{12}, F_{21}, and F_{22} are corresponding (2×2) matrices of e^{AT}, and H_1 and H_2 are corresponding (2×2) matrices of $e^{(AT/2)}BE$. F, H, $i_s(k)$, $\lambda_r(k)$, and $\Delta T(k)$ are the values at the sampling instant of kT. Thus, using (15) and replacing $i_s(k+1)$ with the reference $i_s(k+1)$, the deadbeat control law is given as follows [10]:

$$\Delta T(k) = (H_1)^{-1}[i_s^*(k+1) - F_{11} i_s(k) - F_{12} \lambda_r(k)]. \quad (16)$$

The symbol "*" denotes the reference quantities.

This control law forces the output currents to be exactly equal to the reference signal at the $(k+1)$th sampling instant. To compute (16), the values of F_{11}, F_{12}, and H_1, which are derived from the actual motor speed and plant parameters, have to be calculated or searched from a look-up table, and $i_s(k)$ and $\lambda_r(k)$ must be provided at every sampling instant. The references are one sampling ahead of preview values of stator currents, which are provided by the vector control method. If $i_s(k)$ is detected at kT from which $\lambda_r(k)$ is estimated, followed by computation of (16), then the pulsewidth $\Delta T_{ab}(k)$, $\Delta T_{bc}(k)$, and $\Delta T_{ca}(k)$ cannot be as large as the sampling interval T due to the finite calculation time. To overcome this problem, $i_s(k)$ and $\lambda_r(k)$ are predicted at the $(k-1)$th sampling instant, and (16) is computed before kth sampling instant, which enables the maximum pulse width to be equal to T.

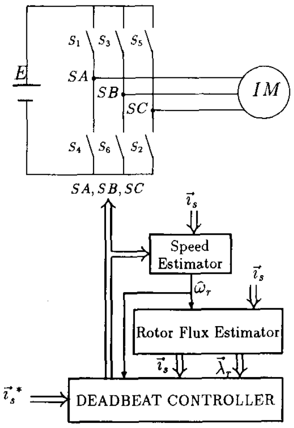

Fig. 2. Proposed digital control system.

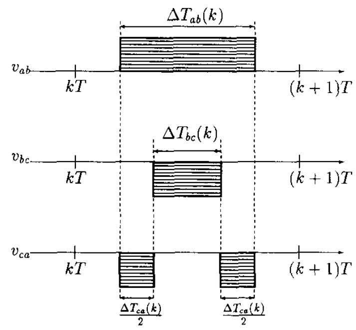

Fig. 3. Pulse pattern selection (example).

C. Pulse Pattern Selection

From $\Delta T_d(k)$ and $\Delta T_q(k)$ obtained in (16), the three-phase pulse pattern $\Delta T_{ab}(k)$, $\Delta T_{bc}(k)$, and $\Delta T_{ca}(k)$ are calculated. The next problem is how to select the actual pulse pattern as shown in Fig. 3, in which $\Delta T_{ca}(k)$ is split into two, however, the other possibility is to divide $\Delta T_{bc}(k)$ and use one pulse of $\Delta T_{ca}(k)$. Also in case of a transient state, the control law (16) sometimes indicates the larger pulse than T. Through this study, the following algorithm is used to select the actual pulse pattern:

1) Each pulse is located symmetrically at the center of the sampling interval.
2) If two of $\Delta T_{ab}(k)$, $\Delta T_{bc}(k)$, and $\Delta T_{ca}(k)$ are the same polarity, compare the absolute values, divide the larger one into two pulses, and keep the rest in one pulse.
3) If at least one of the $\Delta T_{ab}(k)$, $\Delta T_{bc}(k)$, and $\Delta T_{ca}(k)$ exceeds T, then reduce the largest to T and proportionally reduce the others.

This algorithm provides the best results through simultations in Section VI.

IV. Predictive State Observer

A. Design of Observer with Corrective Prediction Error Feedback

The observer state equation with corrective prediction error feedback becomes as follows [7], [8],

$$\begin{bmatrix} \hat{i}_s(k+1) \\ \hat{\lambda}_r(k+1) \end{bmatrix} = \begin{bmatrix} F_{11} & F_{12} \\ F_{21} & F_{22} \end{bmatrix} \begin{bmatrix} \hat{i}_s(k) \\ \hat{\lambda}_r(k) \end{bmatrix} + \begin{bmatrix} H_1 \\ H_2 \end{bmatrix} \Delta T(k) + \begin{bmatrix} G_1 \\ G_2 \end{bmatrix} [i_s(k) - \hat{i}_s(k)]. \quad (17)$$

The symbol "^" denotes the predicted quantities, and

$$G \triangleq \begin{bmatrix} G_1 \\ G_2 \end{bmatrix}$$

is the gain matrix.

The error dynamics of the observer is

$$e(k+1) = (F - GC)e(k) \quad (18)$$

where

$$e(k) \triangleq \begin{bmatrix} i_s(k) - \hat{i}_s(k) \\ \lambda_r(k) - \hat{\lambda}_r(k) \end{bmatrix}. \quad (19)$$

The gain matrix G is designed such that the poles of (18) take the desired values. Thus the pole placement technique is used, in which (15) is first transformed into a controllable canonical form, then four poles of the observer are assigned. With choice of the observer gain matrix G as shown in (20), it is possible to place the poles at any specified conjugate complex pairs in the s domain [9].

$$G_1 \triangleq g_1 I + g_2 J = \begin{bmatrix} g_1 & -g_2 \\ g_2 & g_1 \end{bmatrix}$$
$$G_2 \triangleq g_3 I + g_4 J = \begin{bmatrix} g_3 & -g_4 \\ g_4 & g_3 \end{bmatrix}. \quad (20)$$

The predicted state variables are then used for deadbeat control law in (16), which is transformed into

$$\Delta T(k+1) = (H_1)^{-1} \cdot [i_s(k+2) - F_{11}\hat{i}_s(k+1) - F_{12}\hat{\lambda}_r(k+1)] \quad (21)$$

B. Observer Poles Selection

The selection of the observer poles is a compromise between the rapidity of response of the error and the sensitivity to disturbances and measurement noises. Proceeding by simulations, the observer poles $\alpha_1 \pm j\beta_1$ and $\alpha_2 \pm j\beta_2$, which provided the best result from the viewpoint of overall system performance, were selected, as shown in (22) [14],

$$\begin{aligned} \alpha_1 \pm j\beta_1 &= k_p(\gamma_1 \pm j\gamma_1) \\ \alpha_2 \pm j\beta_2 &= k_p(\gamma_2 \pm j\gamma_2) \end{aligned} \quad (22)$$

where γ_1 and γ_2 are the real parts of the motor poles in (12). k_p is a constant $k_p \leq 4$ and the corresponding Z domain observer poles are given by

$$\begin{aligned} \zeta_1 \pm j\eta_1 &= e^{\alpha_1 T}\cos\beta_1 T \\ \zeta_2 \pm j\eta_2 &= e^{\alpha_2 T}\sin\beta_2 T \end{aligned}. \quad (23)$$

This variable butterworth pattern poles provided the best results through simulations and experiments. Under this choice, the measurement noises effect is greatly reduced.

V. Speed and Voltage Sensorless Field-Oriented Controller

A. Voltage Estimation

Since the stator voltage pulsewidth ΔT is the input to the observer in (17), a voltage sensor is not required. However, in (6) the stator voltage is required for the stator flux estimation. The relation between the stator voltage v_s and the correspondent pulse width ΔT is given by

$$v_s(k) = E\frac{\Delta T(k)}{T}. \quad (24)$$

The use of (24) is valid under two conditions: one is that the dc voltage E is constant, the second one is that the switching devices of the inverter are ideal, or that the switching frequency is very low and the switching time is negligibly short (which is the case for the proposed controller). Otherwise, the stator voltages would have to be sensed and the measured values should be used.

B. Speed Sensorless Field-Oriented Control Scheme

The current reference $i_s^*(k+2)$ is computed by the field orientation, in which the estimated rotor flux $\hat{\lambda}_r(k+1)$, the stator current $\hat{i}_s(k+1)$ from the state observer (17), and the estimated rotor speed $\hat{\omega}_r(k)$ from (11) are used. The block diagram of the proposed voltage and speed sensorless field-oriented control based on the predictive observer with deadbeat response of stator current is shown in Fig. 4, in which the rotor flux reference $|\lambda_r^*|$ and the torque reference T_e are given. Then, first using the estimated stator flux, the rotor speed is identified from (11). Second, the predicted rotor flux and stator current are then computed from (17). Third, the torque- and flux-producing currents are calculated based on the field orientation. Finally, the deadbeat controller calculates the stator voltage pulsewidths. The detailed step by step procedure will be described in Section VIII-C.

VI. Simulations

A. Proposed Controller Simulations

In order to verify the proposed sensorless control law, including speed estimation (11), the deadbeat control law (16), and the state observer (17), digital simulations were

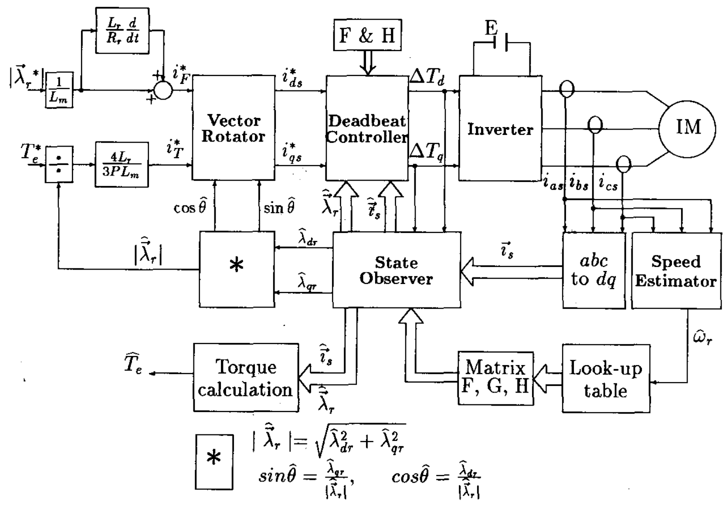

Fig. 4. Block diagram of the proposed system.

carried out. The motor parameters used for simulation are listed in the appendix. Fig. 5 shows the waveform of stator currents, electromagnetic torque, rotor speed, and rotor fluxes under the proposed controller through a reverse speed operation, with the sampling frequency of 1.8 kHz. The waveforms depicted through this figure prove the feasibility of the proposed scheme. The speed is well estimated, the rotor fluxes and stator currents are well predicted, and the deadbeat response is verified. Fig. 6 shows the comparison of torque and currents ripple between the proposed and the conventional hysteresis comparator method in which the phase currents are forced to track the reference generated by the vector controller. The switching frequency of the proposed pulse pattern in Fig. 3 is about two-thirds of the sampling frequency, thus the average of the switching frequency of the hysteresis comparator method is adjusted to be equal to it, which is about 1.2 kHz. From Fig. 6, the torque ripple of the proposed control method is about 40% less than that of hysteresis method.

B. Parameter Sensitivity

The coefficients in (16) and (17) are all dependent on motor parameters. Since these parameters may vary during on-line operation due to temperature or saturation effects, it is important to investigate the sensitivity of the complete system to parameters changes. One of the most significant changes in motor parameters is the rotor resistance R_r. It was shown in [9] that the deadbeat control is not affected by the practical range of R_r change. Note that the sensitivity of the complete system to R_r change increased as the motor speed decreased. To investigate the sensitivity of the predictive observer and its comparison to the conventional slip frequency vector control (in which the rotor flux angle is calculated using rotor speed and slip frequency values), the value of R_r is changed in the motor model. The deadbeat controller is used for both methods. Table I shows that the R_r mismatch causes a large torque deviation in the conventional method (within 20%), whereas the effects in the proposed method is smaller (within 3%). This demonstrates that the proposed observer is very robust against the variation of R_r.

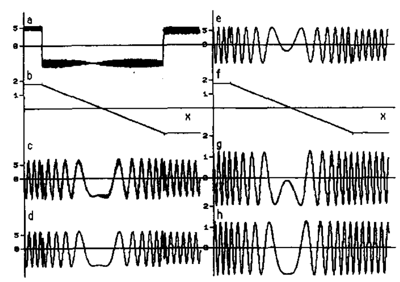

Fig. 5. Reverse speed operation without speed sensor. X = time 0.1 s, $a = T_e^*$, T_e(Nm), $b = \omega_r$, $\hat{\omega}_r$ (r/min), $c = i_{ds}^*$, i_{ds} (A), $d = i_{ds}$, $\hat{i}_{ds}$ (A), $e = i_{qs}$, $\hat{i}_{qs}$ (A), $f = \omega_r$, $\hat{\omega}_r$ (r/min), $g = \lambda_{dr}$, $\hat{\lambda}_{dr}$ (Wb), $h = \lambda_{qr}$, $\hat{\lambda}_{qr}$ (Wb).

VII. Experiments

A. Experimental Setup

Fig. 7 shows a low-power experimental setup for verification of the proposed control scheme. The power MOSFET's are used for switching devices of the inverter bridge. However, the switching frequency in the following experiment is as low as 1.2 kHz, thus the proposed control method will not be deteriorated even if the slower switching devices are used in the high-power systems. The stator currents are detected through Hall-type sensors. Stator currents are sampled and held at every sampling instant, then A/D converted with 2 μs conversion time. The 32-b DSP (NEC μPD77230) performs the field-oriented, deadbeat, and predictive observer calculations as well as data acquisition and PWM pattern selection every 555 μs. The look-up table for coefficients of deadbeat control and variable observer poles as well as the control

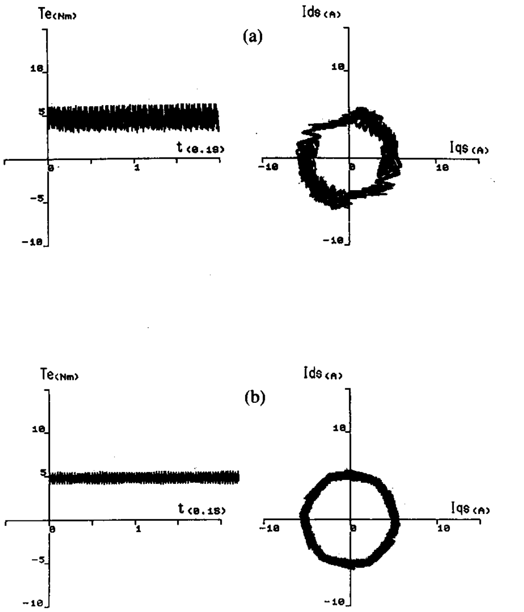

Fig. 6. Comparison of torque and current ripple at 60 Hz operation. (a) Conventional method. (b) Proposed method.

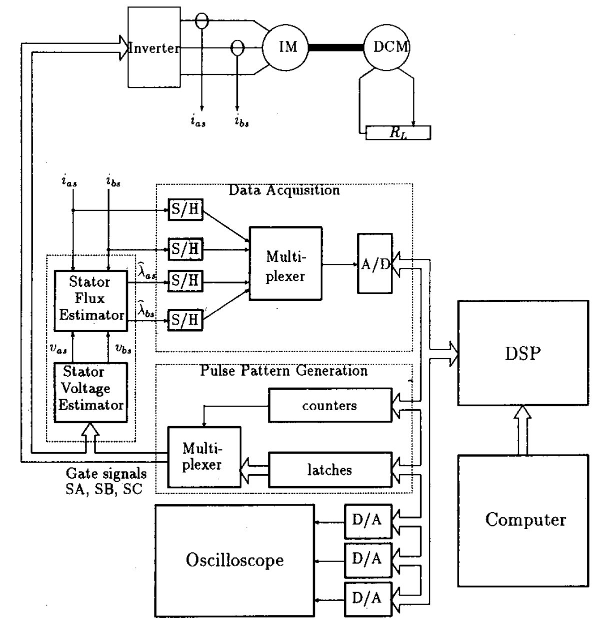

Fig. 7. Controller hardware based on current sensors only.

TABLE I
OBSERVER SENSITIVITY TO PARAMETERS VARIATION: TORQUE VARIATION VERSUS R_r VARIATION ($T_e^* = 5$ Nm, $\omega_r = 1700$ r/min).

R_2/R_2^*	1.05	1.1	1.15	1.2	1.25	1.3	
$\frac{T_e - T_e^*}{T_e^*} \times 100(\%)$	3.75	7.30	9.00	11.20	15.10	19.50	o
$\frac{T_e - T_e^*}{T_e^*} \times 100(\%)$	0.15	0.3	0.90	1.70	2.00	2.30	Δ

o: conventional vector control method.
Δ: proposed method based on predictive observer.

program are storage in 4 kW DSP memory. Receiving the pulse pattern and pulse-widths as binary data, the custom-made pulse distribution board generates the gate signals to six FET's. Three D/A converters are used to display the desired signals. A dc motor is used as the system load.

B. Flux Integration

The success of the speed sensorless system depends on good estimation of the stator flux angle, based on (6), which is difficult to implement because of the pure integration of the stator phase voltage minus the voltage drop in the stator resistance. This leads to problem with initial conditions and drift. In fact, the estimator is only required to calculate the synchronous speed, ω, that is, the variation of stator flux angle. This means that the used quantities in the observer need not to be the actual stator flux components but can be auxiliary variables related to them. Therefore, the undesirable integral function is removed, and a low-pass filter with very low cutting frequency, is used. This also attenuates the high-frequency components normally found in the motor terminal voltages. On the other hand, the dc offset must be eliminated to prevent saturation of the integrator. In the implementation of stator flux estimation, a high-pass filter with very low cutting frequency is added.

The "integration" of the stator flux was done by analog hardware. The stator voltage is reconstructed from the inverter switching states. The algorithm of the stator voltage v_s estimation is as follows [13]. A switching function SA for phase A of the innverter shown in Fig. 2 is first defined:

SA = 1: when upper switch of phase A is on

SA = 0: when lower switch of phase A is on

A similar definition is adopted for phases B and C. The stator phase voltages can be given in terms of switching states and the dc voltage E as follows:

$$v_{as} = \frac{E}{3}(2 \times \mathrm{SA} - \mathrm{SB} - \mathrm{SC})$$
$$v_{bs} = \frac{E}{3}(-\mathrm{SA} + 2 \times \mathrm{SB} - \mathrm{SC})$$
$$v_{cs} = \frac{E}{3}(-\mathrm{SA} - \mathrm{SB} + 2 \times \mathrm{SC}). \quad (25)$$

Note that SA, SB, and SC are the outputted pulses of the DSP. As the speed decreases, the pulseswidth becomes very small, therefore the deadtime of the power MOSFET's is no longer negligible. The effect of this turn-on-off time. as well as the effect of the stator resistance has to be compensated to allow the speed sensorless system to work at very low speed. This is beyond the scope of this paper. On the other hand, the dc link voltage E was theoretically supposed constant. However, in the actual experimental test fluctuations of up to 2% of the rated value E do not affect the controller performance.

As Fig. 7 shows, the sensors, which collect information directly from the induction motor, are current sensors, although an additional sample holder are required for the analog estimation of the stator flux. The estimated stator fluxes are sampled holded, and A/D converted at every sampling instant, from which the rotor speed is computed, and used instead of the measured one.

C. Software

The following step-by-step strategy is employed to realize the proposed control law.

1) Set the rotor flux reference $|\lambda_r^*|$ and the torque reference T_e^* at selected values.

2) The stator flux estimator (analog technique) is

$$\lambda_s = \int (v_s - R_s i_s)\,dt \tag{26}$$

3) Data inputs are

a) A/D conversion of stator currents is $i_{as}(k)$ and $i_{bs}(k)$.

$$i_s(k) = \begin{bmatrix} i_{ds}(k) \\ i_{qs}(k) \end{bmatrix} = \frac{2}{3}\begin{bmatrix} \frac{3}{2} & 0 \\ \frac{\sqrt{3}}{2} & \sqrt{3} \end{bmatrix}\begin{bmatrix} i_{as}(k) \\ i_{bs}(k) \end{bmatrix}. \tag{27}$$

b) A/D conversion of stator fluxes is $\hat{\lambda}_{as}(k)$ and $\hat{\lambda}_{bs}(k)$.

$$\lambda_s(k) = \begin{bmatrix} \hat{\lambda}_{ds}(k) \\ \hat{\lambda}_{qs}(k) \end{bmatrix} = \frac{2}{3}\begin{bmatrix} \frac{3}{2} & 0 \\ \frac{\sqrt{3}}{2} & \sqrt{3} \end{bmatrix}\begin{bmatrix} \hat{\lambda}_{as}(k) \\ \hat{\lambda}_{bs}(k) \end{bmatrix}. \tag{28}$$

4) Rotor speed identification:

a) Rotor speed is

$$\hat{\omega}_r(k) = \frac{\hat{\lambda}_{ds}(k-1)\hat{\lambda}_{qs}(k) - \hat{\lambda}_{qs}(k-1)\hat{\lambda}_{ds}(k)}{tT(\hat{\lambda}_{ds}^2 + \hat{\lambda}_{qs}^2)} - \frac{4R_r}{3P}\frac{Te^*}{(|\vec{\lambda}_r^*|)^2}. \tag{29}$$

b) Look-up table, matrices $F = F(\hat{\omega}_r(k))$, $G = G(\hat{\omega}_r(k))$, and $H = H(\hat{\omega}_r(k))$.

5) Predictive observer:

$$\begin{bmatrix} \hat{i}_s(k+1) \\ \hat{\lambda}_r(k+1) \end{bmatrix} = \begin{bmatrix} F_{11} & F_{12} \\ F_{21} & F_{22} \end{bmatrix}\begin{bmatrix} \hat{i}_s(k) \\ \hat{\lambda}_r(k) \end{bmatrix} + \begin{bmatrix} H_1 \\ H_2 \end{bmatrix}\Delta T(k) + \begin{bmatrix} G_1 \\ G_2 \end{bmatrix}[i_s(k) - \hat{i}_s(k)]. \tag{30}$$

6) Field-oriented control:

a) The rotor flux magnitude is

$$|\hat{\lambda}_r(k+1)| = \sqrt{\hat{\lambda}_{dr}(k+1)^2 + \hat{\lambda}_{qr}(k+1)^2}. \tag{31}$$

b) The flux producing current is

$$i_F^* \triangleq \frac{|\lambda_r^*|}{L_m}. \tag{32}$$

c) The torque-producing current is

$$i_T^* \triangleq \frac{4}{3P}\frac{L_r}{L_m}\frac{T_e^*}{|\hat{\lambda}_r(k+1)|}. \tag{33}$$

d) The rotor flux angle is

$$\hat{\varphi}_{(k+1)} \triangleq \tan^{-1}\left(\frac{\hat{\lambda}_{qr}(k+1)}{\hat{\lambda}_{dr}(k+1)}\right)$$

$$\Delta\hat{\varphi}_{(k+1)} \triangleq \hat{\varphi}_{(k+1)} - \hat{\varphi}_{(k)}$$

$$\hat{\theta} \triangleq \hat{\varphi}_{(k+2)} \triangleq \hat{\varphi}_{(k+1)} + \Delta\hat{\varphi}_{(k+1)}. \tag{34}$$

e) Current references are

$$i_s^*(k+2) \triangleq \begin{bmatrix} i_{ds}^*(k+2) \\ i_{qs}^*(k+2) \end{bmatrix} \triangleq \begin{bmatrix} \cos\hat{\theta} & -\sin\hat{\theta} \\ \sin\hat{\theta} & \cos\hat{\theta} \end{bmatrix}\begin{bmatrix} i_F^* \\ i_T^* \end{bmatrix}. \tag{35}$$

7) Deadbeat control law:

$$\Delta T(k+1) = (H_1)^{-1}[i_s^*(k+2) - F_{11}\hat{i}_s(k+1) - F_{12}\hat{\lambda}_r(k+1)]. \tag{36}$$

8) Pulse pattern selection.

9) Output control at the right moment.

D. Experimental Results

With the aforementioned hardware and software, speed and voltage sensorless field-oriented control based on predictive observer with deadbeat response of stator currents was carried out. Fig. 8(a) shows the waveforms of the stator currents and its reference. It is verified that the expected deadbeat response is achieved, which means that the speed estimator and the state observer results correlate with the real values.

The waveforms of the predicted and actual torque at 60 Hz operation under the open-loop control of the stator current (in which a sinusoidal PWM stator voltages are applied to the induction motor), and under the deadbeat control are shown in Fig. 8(b). The down arrow shows the switching instant from the open-loop control to the deadbeat one. The predicted torque is given as follows:

$$\hat{T}_e(k+1) = \frac{3P}{4}\frac{L_m}{L_r}[\hat{i}_{qs}(k+1)\hat{\lambda}_{dr}(k+1) - \hat{i}_{ds}(k+1)\hat{\lambda}_{qr}(k+1)]. \tag{37}$$

Assuming that the rotor flux vector is well estimated by the observer, the actual torque in Fig. 8(b) is given by

$$T_e(k) = \frac{3P}{4}\frac{L_m}{L_r}(i_{qs}(k)\hat{\lambda}_{dr}(k) - i_{ds}(k)\hat{\lambda}_{qr}(k)). \tag{38}$$

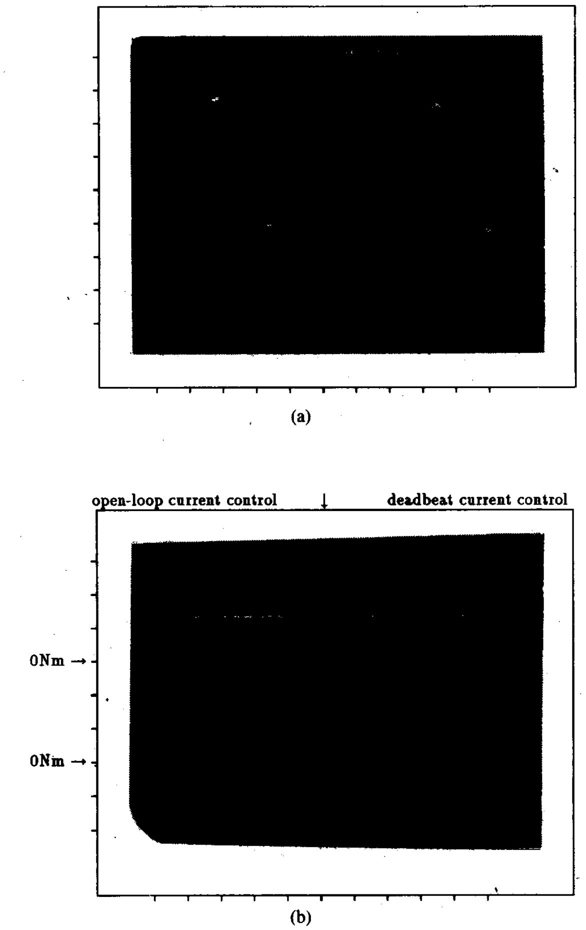

Fig. 8. Steady state characteristics at 60 Hz operation. (a) Actual (upper) and reference (lower) currents: 3 A/div, 5 ms/div. (b) Actual (lower) and predicted (upper) torque: 3 Nm/div, 0.2 s/div.

Equations (37) and (38) are computed in DSP and output through D/A converters. The torque ripples with the deadbeat control are smaller than those with the open-loop control.

Fig. 9 shows the transient operation from 100 to 700 r/min by changing the torque reference. Reference and actual currents as well as estimated and actual rotor speed depicted in these figures, indicate that the proposed drive performance is satisfactory at transient operation. The actual rotor speed is detected by a pulse generator (5000 ppr) and the pulses are counted by 16-b counters. The calculated speed is D/A output in the picture. The low rotor-speed ($\omega_r = 100$ r/min with 4 Hz) operation is illustrated in Fig. 10, which is realized under the variable poles placement of the state observer [9].

VIII. Conclusions

A fully digital scheme to control induction motor stator currents under speed and voltage sensorless field-oriented system, based on deadbeat control theory and a predictive

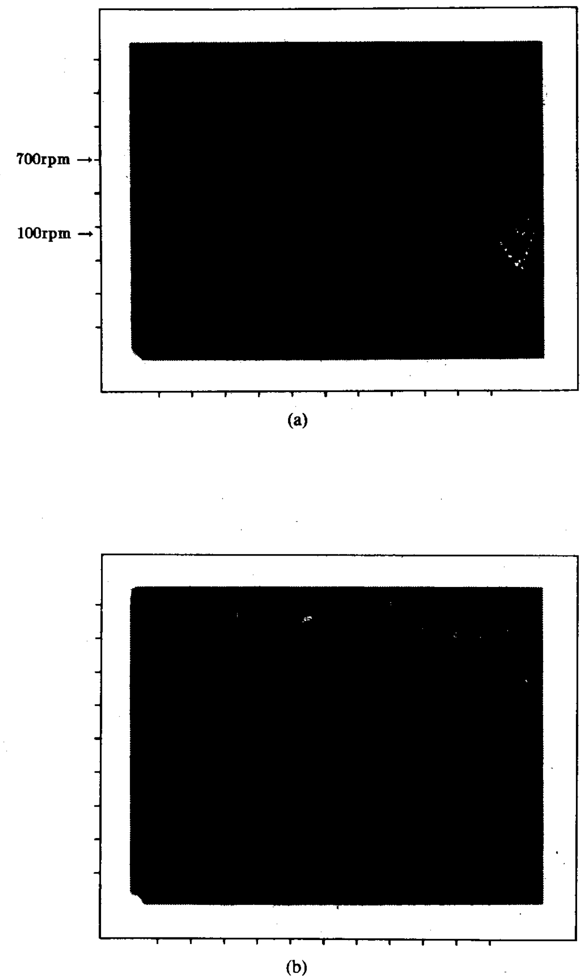

Fig. 9. Transient characteristics from 100 r/min to 700 r/min. (a) Actual (lower) and estimated (upper) speed: 1 s/div. (b) Actual (upper) and reference (lower) currents: 2 A/div, 0.1 s/div.

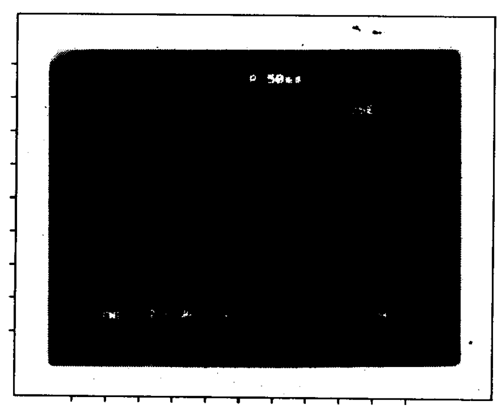

Fig. 10. Steady-state characteristics of 4 Hz operation. Actual (upper) and reference (lower) currents: 2 A/div, 50 ms/div.

state observer, was proposed. The rotor speed is identified with less sensitivity to parameters variation than the conventional method. The deadbeat controller enabled a low-current ripple with lower switching frequency, which, in turn, resulted in low-torque ripple. The predictive state observer made possible the estimation of rotor flux with very low sensitivity to parameters variation. The stator voltage is estimated. As a result, only current sensors are used for the implementation of the system drive. The authors believe the proposed digital control scheme for the induction motor will cultivate the possibility of new high-performance torque control approach.

Appendix

Induction motor parameters: 0.75 kW, three phases, 60 Hz, four poles, 200 V

$R_s = 3.3534\ \Omega$, $R_r = 1.9913\ \Omega$

$L_s = 170.67$ mH, $L_r = 170.67$ mH,

$L_m = 163.73$ mH

References

[1] C. Schauder, "Adaptive speed identification for vector control of induction motors without rotational transducers," in *Proc. IEEE-IAS Annu. Meet.*, 1989, pp. 493–499.

[2] A. Fratta, A. Vagati, and F. Villata, "Vector control of induction motors without shaft transducers," in *Proc. IEEE PESC Conf. Rec.*, 1988, pp. 839–846.

[3] H. Nakano and I. Takahashi, "Speed sensorless field oriented control of an induction motor using an instantaneous slip frequency estimation method," in *Proc. IEEE PESC Conf. Rec.*, 1988, pp. 847–854.

[4] S. Tamai, H. Sugimoto, and M. Yano, "Speed sensorless vector control of induction motor applied model reference adaptive system," in *Proc IEEE IAS Conf. Rec.*, 1985, pp. 613–620.

[5] X. Xu, R. DeDoncker, and D. W. Novotny, "A stator flux oriented induction machine drive," in *Proc. IEEE PESC Conf. Rec.*, 1988, pp. 870–876.

[6] B. K. Bose, "Technology trends in microcomputer control of electrical machines," *IEEE Trans. Ind. Electron.*, vol. 35, no. 1, pp. 160–177, 1988.

[7] G. Verghese and S. Sanders, "Observers for fast flux estimation in induction machines," in *Proc. IEEE Power Electron. Spec. Conf. Rec.*, 1985, pp. 751–760.

[8] H. Hashimoto, Y. Ohno, S. Kondo, and F. Harashima, "Torque control of induction motor using predictive observer," in *Proc. IEEE Power Eleetron. Spec. Conf.*, 1989, pp. 271–274.

[9] A. Kawamura and L. Ben-Brahim, "Deadbeat control of induction motor current using state observer with adaptive poles selection," *Trans. IEE Japan*, vol. 108-D, no. 5, pp. 590–597, May, 1990.

[10] L. Ben-Brahim and A. Kawamura, "Digital control of induction motor current using predictive state observer," in *Proc. IPEC*, 1990, pp. 489–496.

[11] L. Ben-Brahim and A. Kawamura, "Digital current regulation of field oriented controlled induction motor based on predictive flux observer." *IEEE Trans. Industry Applications*, vol. 27, no. 5, pp. 956–961, Sept./Oct. 1991.

[12] L. Ben-Brahim and A. Kawamura, "Speed and voltage sensorless field oriented control of induction motor based on observer with digital current regulation," in *Proc. IEE of Japan IAS Annu. Meet.*, pp. I.124–I.132, Aug. 1990.

[13] T. G. Habetler and D. M. Divan, "Control strategies for direct torque control using discrete pulse modulation," in *Proc. IEEE IAS Annu. Meet.*, Oct. 1989, pp. 514–522.

[14] L. Ben-Brahmin, "High performance torque control of induction motor based on digitally controlled PWM inverter," Ph.D. dissertation, Department of Electrical and Computer Engineering, Yokohama National University, Yokohama, Japan, Dec. 1991.